24th European Rotorcraft Forum
Marseilles, France, 15th - 17th September, 1998

Numerical Detection of Blade-Vortex Interactions Using a Free Wake Analysis - A Comparison of Various Approaches

AE10

Lionel TAUSZIG* and Farhan GANDHI**

Rotorcraft Center of Excellence
Department of Aerospace Engineering
The Pennsylvania State University
233 Hammond Building
University Park, PA 16802, USA

The present study compares BVI predictions obtained using a free-wake analysis and 5 different BVI detection methods - *(i)* planar method, *(ii)* spherical method, *(iii)* inflow, *(iv)* blade loads, and *(v)* blade root loads. The results indicate that the planar method is ill-suited for detection of parallel BVI, requiring a very high-resolution azimuthal discretization and considerable post-processing of wake data. The spherical method is well-suited for detection of parallel BVI and is effective even with a moderate- to low-resolution azimuthal discretization. Detection of BVI based on inflow or blade loads will be unsuccessful if the vortex core radius is too large. However, if the vortex core is reasonably "tight", impulsive changes in inflow and blade loads can be identified even with a moderate-resolution azimuthal discretization. For a sufficiently "tight" vortex core, observed impulsive changes in blade root loads can be linked to the occurrence of parallel BVI events.

1. Introduction

The interactions between helicopter main rotor blades and the strong tip vortices dominating the rotor wake - known as Blade-Vortex Interactions (BVI) - can result in impulsive blade loads that produce significant vibration and noise. BVI is a particularly serious problem in low speed and descending flight conditions when the tip vortices remain in close proximity of the rotor. Alleviation of BVI noise would significantly decrease the current resistance to operation of rotary-wing aircraft in populated areas, and open up a potentially large commercial market for helicopters and tilt-rotors as the vehicles of choice for transportation to, and from, city centers. On the military side, alleviation of BVI noise is important for reduction of detectability. The reduction of vibrations associated with BVI would decrease crew, passenger, as well as structural component fatigue - for both military and civilian helicopters. Due to the above reasons, significant efforts have been devoted over the last several years toward the alleviation of BVI [1]. These efforts have included examining various passive blade designs (such as advanced tip configurations), active control concepts (such as Higher Harmonic Control, Individual Blade Control, and Trailing Edge Flaps), and operational methods.

Irrespective of the approach chosen to reduce BVI, it is important, first, to accurately predict the harmful interactions of the baseline configuration, and then determine the effect that the proposed design changes or control schemes would produce on the BVI characteristics. A preliminary design phase involving broad parametric studies on the effectiveness of the concept under consideration is generally based on numerical simulations; with expensive tests usually conducted at fairly advanced stages in the development. Thus, the importance of accurate numerical detection of blade-vortex

* Graduate Research Assistant, Member AHS
** Assistant Professor, Member AHS, AIAA
Proceedings of the 24th European Rotorcraft Forum, Marseilles, France, September 15-17, 1998

interactions in evaluating the feasibility and scope of new passive designs, active control schemes, or operational concepts, cannot be over-emphasized.

Numerical detection of BVI requires - *(i)* a description of the distorted rotor wake, *(ii)* a description of the blade motions, and *(iii)* a scheme to identify the occurrence of BVI events. The solution of the rotor wake and blade response problem is inherently coupled, as one affects the other. BVI identification schemes often involve post-processing of the rotor wake and blade response calculations. For numerical simulations of the rotor wake, two possible approaches are - *(i)* use of CFD (Navier-Stokes or Euler formulations), or *(ii)* use of free-wake analyses. The second approach is more attractive from the standpoint of considerably lower computational requirement. Additionally, the use of CFD approaches are plagued with problems such as numerical dissipation, and are unable, at the present time, to provide accurate descriptions of the tip vortices at the required distances downstream. Consequently, many researchers have used free-wake analyses as a stepping-stone for numerical detection and characterization of blade-vortex interactions.

Several approaches have been used to numerically detect BVI. Some of these are based on calculating the inflow at the blade, the lift, or a geometric parameter such as the "miss distance". However, while an individual researcher may have used a particular approach for BVI detection, no unified study conducting a side-by-side examination of the effectiveness of the various methods - including a comparison of their inherent strengths, limitations, and computational costs - is available in the literature. Such a study is important to understand the relative merits and shortcomings of the various detection methods, and to develop an appreciation of "what it takes" to successfully detect BVI using a particular method.

In the present study, BVI predictions using five different methods are compared. The criteria used are - *(i)* planar detection or "miss-distance"; *(ii)* spherical detection (a new approach developed by the authors); *(iii)* inflow; *(iv)* blade loads; and *(v)* blade root loads. Based on the results presented in the paper, conclusions are drawn on the ability of each criteria to detect parallel BVI, the azimuthal discretization required, the post-processing or computational overhead involved in each case, and the influence of vortex core size on the BVI predictions.

2. Free-Wake Analysis for Detection of BVI

The free-wake analysis used in the present study is based on the formulation of the Maryland Free Wake (MFW) described in Refs. [2, 3]. However, the formulation was independently coded and implemented at the Pennsylvania State University [4]. It uses a relaxation approach wherein the tip-vortex filaments constituting the far wake are allowed to convect under the influence of the local velocity (comprising the free-stream velocity as well as the self- and mutually-induced velocities due to all the vortex filaments in the wake) to assume a distorted wake geometry. For the solution of the distorted wake geometry, the wake is discretized in space (ζ) and time (ψ), as shown in Fig. 1. The spatial discretization approximates the tip vortices by segments (of length $\Delta\zeta$) with "collocation points" at the ends of the segments. Thus, evaluation of the distorted wake geometry implies determining the coordinates of the collocation points on the tip vortex, at several discrete azimuthal locations. For the simulations in the present study, the spatial step size used is $\Delta\zeta = 9°$, with the tip vortices extending up to four rotor revolutions. The temporal or azimuthal step size used is $\Delta\psi_{wake} = 4.5°$, implying that the free-wake geometry is determined at $N_{wake} = 80$ azimuthal grid points. This *low-resolution* azimuthal grid, while facilitating computation of the free-wake geometry at a reasonable cost, is generally regarded as inadequate for detection of BVI. The partial differential equations governing the motion of vortex filaments (or collocation points) in the wake are solved, after discretization, using a pseudo-implicit predictor-corrector algorithm with a five-point central difference scheme (described in Refs. [2, 3, 4]).

Evaluation of the free-wake geometry is coupled to the solution of the blade flapping response and rotor trim. This is because the distortion of the wake geometry influences the

inflow and airloads at the blade, which in turn influence the wake geometry via blade flapping, change in blade circulation or lift, and change in strength of the tip vortices. For the determination of the blade flapping response, the airloads must be calculated around the azimuth. In the present study, the azimuth is discretized into N_{trim} = 160 grid points (corresponding to a step size of $\Delta\psi_{trim}$ = 2.25°), at which the inflow and the blade loading are computed. This *moderate-resolution* grid overlaps the low-resolution free-wake grid. Since the wake geometry is evaluated only at the N_{wake} = 80 points of the low-resolution grid, interpolation of the geometry is required in order to compute the inflow and blade loads at the intermediate points of the moderate-resolution grid. In the present free-wake implementation, this moderate-resolution grid is used (rather than the low-resolution free-wake grid) for blade response and trim calculations, as it can better represent impulsive changes in flap response that may occur due to parallel BVI, or allow introduction of non-harmonic or impulsive changes in blade pitch input to control BVI. For detection of parallel BVI, a *high-resolution* azimuthal discretization is usually required. In the present study, a high-resolution grid comprising of N_{BVI} = 640 azimuthal steps is used (corresponding to a step size of $\Delta\psi_{BVI} \approx$ 0.56°). The distorted wake geometry corresponding to any point on the high-resolution grid is once again obtained by interpolating the geometry evaluated at the low-resolution free-wake grid points. Such an interpolation approach of free-wake geometry onto a high-resolution BVI detection grid has been previously used by other researchers, Refs. [5, 6]. In addition to using the high-resolution grid, the use of moderate- and low-resolution grids for detection of parallel BVI are also considered in the present study.

The computation of the distorted wake geometry is susceptible to numerical singularity problems associated with very high velocities of the tip vortices. To alleviate these problems a viscous core model is usually introduced. Following Refs. [2, 3, 7], the viscous core of the vortex is assumed to grow as follows:

$$r_c(\zeta) = 2.24\sqrt{\nu\delta\frac{\zeta}{\Omega}} \qquad (1)$$

where ν is the kinematic viscosity of air, and δ is an "eddy" or turbulent viscosity coefficient. For δ = 1 (representing a laminar vortex) the diffusion of the vortex is much slower than that observed experimentally. The turbulent viscosity factor is thus introduced to simulate the significantly faster growth rate of the core of a real vortex, and its value is generally selected empirically. In Refs. [2, 3], a value of δ of the order of 10^4 was used. This was based on the following expression relating the turbulent viscosity coefficient to the vortex Reynolds number, Γ/ν:

$$\delta = 1 + a_1\frac{\Gamma}{\nu} \qquad (2)$$

with a value of 0.1 selected for the empirical coefficient, a_1. In Ref. [3] this value of a_1 = 0.1 was recommended as it was reported to produce the most physically accurate distorted wake geometry, and this value is nominally retained in the present study. However, in section 7, the impact of using varying core growth rates (varying values of a_1) is examined.

3. Description of Model Rotor on which BVI detection is conducted

The free-wake analysis implemented at Penn State University was validated using inflow data, wake geometry data, and BVI measurements [4]. In the present study, effectiveness of various numerical detection methods in identifying the occurrence of parallel blade-vortex interactions is examined using the specifications of a UH-60 model rotor which was tested in the NASA Langley 4x7 meter tunnel, Ref [8]. In Ref. [8], acoustic measurements of BVI noise were reported for a number of different advance ratios and longitudinal shaft angles. BVI predictions using the present free-wake and the spherical detection method (described in section 5) have already been validated against this experimental data, [4], for the different flight conditions tested in Ref. [8]. In the present study, the different detection methods were

used to compare BVI predictions for only one of the flight conditions tested. The flight condition selected corresponded to a moderate speed descent with an advance ratio of 0.14 and a backward shaft tilt of $4.1°$.

4. Planar Detection or Miss-Distance Method

The planar detection method, based on an analogy with laser sheet experiments, defines a plane containing the blade and the rotor shaft and records a BVI event when a tip vortex segment intersects this plane within some specified distance, $\bar{h}$, above or below the blade (Fig. 2). In such an event, the distance between the blade and the intersection point of the vortex segment on the blade-shaft plane is commonly called the "miss-distance", h (Fig. 2).

Implementation of this BVI detection method requires further post-processing of the wake after the distorted wake geometry is obtained by interpolation at the N_{BVI} points of the high-resolution grid. At each of the N_{BVI} azimuthal locations, the positions of the tip-vortices, relative to the blade, are examined. To do so, the tip-vortex collocation points, (x_k, y_k, z_k), are first expressed in cylindrical coordinates, (r_k, ψ_k, z_k), where,

$$r_k = \sqrt{x_k^2 + y_k^2} \quad \text{and} \quad \psi_k = \tan^{-1}\left(\frac{y_k}{x_k}\right) \qquad (3)$$

Next, to identify the tip-vortex segments that intersect the blade-shaft plane (at an azimuthal station denoted as ψ_b), pairs of adjacent collocation points, k and k+1, are successively considered and the quantities $(\psi_b - \psi_k)$ and $(\psi_b - \psi_{k+1})$ are evaluated. If

$$(\psi_b - \psi_k)(\psi_b - \psi_{k+1}) < 0 \qquad (4)$$

this implies that the quantities $(\psi_b - \psi_k)$ and $(\psi_b - \psi_{k+1})$ are of opposite sign, thereby placing the adjacent collocation points on opposite sides of the blade-shaft plane at ψ_b. The radial location, r, and vertical location, z, of the intersection point of the vortex segment on the blade-shaft plane is then determined as follows:

$$r = \frac{(r_k - r_{k+1})}{(\psi_k - \psi_{k+1})}\psi_b + \frac{(r_{k+1}\psi_k - r_k\psi_{k+1})}{(\psi_k - \psi_{k+1})}$$
$$z = \frac{(z_k - z_{k+1})}{(\psi_k - \psi_{k+1})}\psi_b + \frac{(z_{k+1}\psi_k - z_k\psi_{k+1})}{(\psi_k - \psi_{k+1})} \qquad (5)$$

Then, for a blade flapping angle, β, if

$$h = |r\beta(\psi_b) - z| \le \bar{h} \qquad (6)$$

a BVI event is recorded at the azimuth, ψ_b, and radial location, r, with a miss-distance, h. In the present study, a nominal value of $\bar{h} = 3$ chord lengths is used.

If a collocation point, k, happens to fall *on* the blade-shaft plane ($\psi_k \equiv \psi_b$), and satisfies the condition, $h = |r_k\beta(\psi_b) - z_k| \le \bar{h}$, a BVI event is again recorded at the azimuth, ψ_b, and radial location, r_k, with a miss-distance, h.

It should be emphasized that when the blade is at an azimuthal location, ψ_b, every vortex segment (from the tip vortices of all the blades) is examined to determine whether any BVI will occur *at that particular azimuthal location*, ψ_b. This procedure is then repeated at each of the N_{BVI} steps of the high-resolution grid. The effectiveness of the planar detection method in identifying parallel BVI is heavily dependent on the number of azimuthal steps used. To better understand this dependence on number of azimuthal grid points, it is first important to realize that since the azimuth is discretized into a finite number of stations, and BVI detection is being conducted only at these finite stations, some azimuthal discretization error is inevitable. Theoretically, if a perfectly parallel blade-vortex interaction was to occur, the planar detection method would almost certainly be unable to detect it, *irrespective of the number of azimuthal grid points used*. This principle is conceptually illustrated in Fig. 3 which shows the blade at two successive azimuthal stations at which the detection method is implemented, as well as a tip vortex lying along a radial direction (which would produce a parallel BVI) somewhere between these two blade stations. If Eq. 4 was used for BVI

detection at either of the blade locations, j or j+1, the test would produce a negative result since the adjacent collocation points lie on the same side of the blade-shaft plane. Even if the resolution of the grid used is now doubled, resulting in the introduction of an additional intermediate grid point, j+1/2, the planar detection method would again produce a negative result at this intermediate grid point since the collocation points still lie on only one side of the blade-shaft plane, without intersecting it. In practice, of course, the tip vortex never assumes a perfectly radial geometry as shown in Fig. 3. Even in a parallel interaction, the slight obliqueness or curvature of the vortices relative to the blade-shaft planes at which the detection method is implemented (Fig. 3) allows the identification of interactions, especially if a high-resolution azimuthal discretization is used.

Figure 4 shows the blade-vortex interactions predicted using the planar detection method implemented on a high-resolution mesh comprising of N_{BVI} = 640 azimuthal grid points. Although the individual symbols in the figure only represent the occurrence of a BVI event at that particular location, the bands generated by symbols in close proximity provide a fairly good representation of the passage of tip-vortices close to the blade *as it undergoes one revolution*. It should thus be emphasized that the figure is different from a conventional "top view" of the rotor wake, corresponding to a snapshot of the tip vortices at a given instant in time, with the blade frozen at a single azimuthal location. The colors used in the figure have a special significance - green signifies that the vortex is below the blade, blue signifies that the vortex is above the blade, red signifies the vortex passing right through the blade, and darker colors indicate that the vortex is closer to the blade (smaller miss-distance, h). Thus, on the advancing side the vortices can be seen coming from the front of the disk and below the blade, and passing toward the rear of the disk and above the blade.

From Fig. 4, perpendicular interactions can clearly be seen occurring on the front of the disk, while parallel interactions are detected on the advancing and retreating sides. Of the parallel interactions marked I, II, and III, on the advancing side, the interaction II (occurring around $\psi_b = 60°$) appears to be the most parallel and is thus likely to have the largest contribution to BVI noise. Of the interactions IV and V, on the retreating side, the interaction V (occurring around $\psi_b = 300°$) appears more parallel and could potentially have a large contribution to BVI noise.

Figures 5a and 5b, respectively, shows the blade-vortex interactions predicted using the planar detection method implemented on the moderate-resolution mesh comprising of N_{trim} = 160 azimuthal grid points, and on the low-resolution mesh comprising of N_{wake} = 80 azimuthal grid points. As compared to Fig. 4, it is seen that the criteria implemented at 160 and 80 azimuthal grid points has least success in detecting the most parallel interactions, II and V, whereas detection of the perpendicular interactions at the front and the back of the disk is relatively unaffected. Comparing Figs. 4 and 5 clearly illustrates that the effectiveness of the planar detection criteria in identifying the occurrence of the most parallel interactions decreases as the number of azimuthal grid points is reduced.

The planar detection method described in this section will generally be effective in detecting parallel BVI events if a very high-resolution discretization of the azimuth is used. However, the computational overhead associated with the implementation of this method increases with an increase in the number of azimuthal grid points due to interpolation of wake geometry and the post-processing of the rotor wake data required, as described earlier in this section.

5. Spherical Detection Method

This is a new detection method developed by the authors. Unlike the planar detection method, the spherical detection method is not based on an experimental analogy, but can potentially exploit computations that were already carried out in the evaluation of the free-wake geometry. Thus, post-processing of rotor wake data and associated computational overhead may possibly be alleviated. As explained in section 2, determination of the free-wake geometry is coupled with the evaluation of the blade flapping response and

rotor trim. Evaluation of blade flapping response requires rotor blade loads to be calculated as the blade undergoes one revolution. Typically, blade loads are calculated at several discrete equi-distant azimuthal and radial stations. In the present study, loads are evaluated at 15 radial stations along the blade length. These radial stations are called "control points". To calculate the loads at any given control point, the contribution of every tip-vortex segment to the inflow at that control point is considered using the Biot-Savart law. Using the Biot-Savart law to obtain the induced velocity due to a tip-vortex segment requires the calculation of the distance between the control point and that vortex segment. If the distance, r_{mid}, between the control point and mid-point of any vortex segment is less than a user specified distance, $\bar{r}$, a BVI event is recorded at that control point.

This detection criteria can be physically visualized as follows. Control spheres of radii, $\bar{r}$, are constructed about every control point along the blade span. If the mid-point of any vortex segment should come within any of these control spheres (Fig. 6), a BVI event is recorded. Hence the name "spherical detection method".

The spherical detection method is based on discretization in both the radial as well as azimuthal directions (unlike the planar detection method which required discretization along the azimuthal direction alone). Thus, it would appear that the spherical detection method is inferior, since discretization errors along both the azimuth as well as the radius could be expected. As in the case of the planar detection method, the success of the present method would be expected to depend on the azimuthal discretization used. Additionally, however, the radius of the control spheres, $\bar{r}$, is an important parameter. Consider a typical blade of radius approximately 15 - 20 times the chord length. Thus, the 15 control points would be placed approximately 1 - 1.3 chord lengths apart. If the radius, $\bar{r}$, of the control spheres is taken to be equal to one chord length (the value used in the present study), the control spheres would overlap (as shown in Fig. 7a). Thus, at a given azimuthal location, ψ_b, even if a vortex intersected the blade in a perpendicular fashion at a radial location between two control points (marked "XX" in Fig. 7a), the interaction would be detected by the present criteria. To detect a vortex located at "YY" control spheres of larger radii may be used. Thus, discretization errors in the radial direction are not expected to have a serious negative impact on the effectiveness of the spherical detection method.

More significantly, the spherical detection method is much more effective than the planar detection method in detecting the parallel blade-vortex interactions most responsible for the impulsive loading that produce BVI noise and vibration. As explained in the previous section (using Fig. 3), the planar detection method would have considerable difficulty in identifying the occurrence of perfectly parallel interactions due to the fact that the method only examines for interactions on blade-shaft planes at a finite number of azimuthal locations. In contrast, even though the spherical detection method is also implemented only at discrete azimuthal locations, it can be seen from Fig. 7b that the use of control spheres enables the detection of vortices lying between the azimuthal steps.

Figure 8 shows the blade-vortex interactions predicted using the spherical method with a high-resolution mesh comprising of N_{BVI} = 640 azimuthal grid points. The individual symbols in the figure strictly indicate the presence of a vortex element in proximity of the blade at that particular location. However, the bands generated by symbols in close proximity provide a fairly good representation of the passage of tip-vortices close to the blade as it undergoes one revolution. The colors used in the figure have the following significance - as in Figs. 4, 5a, and 5b, darker colors indicate a smaller distance between the mid-point of a vortical segment and the control point (lower value of r_{mid}), green signifies that the vortex is below the blade, blue signifies that the vortex is above the blade, and red signifies the vortex passing right through the blade. As with the planar detection method, vortices can be seen coming from the front of the disk and below the blade, and passing toward the rear of the disk and above the blade, on the advancing side. It is interesting to note that while the interaction IV shows a vortex coming from below the blade (green) and passing above it (blue), it is not explicitly seen passing through the blade

(absence of any red). Similarly, for the interactions I, II, III, and V, passage of the vortex through the blade is not as clearly evident as seen in Fig. 4 (using planar detection method). This can be attributed to discretization errors in the radial direction associated with the spherical detection method. It is likely that the vortex may be intersecting the blade at a radial location between two control points. However, at the two adjacent control points on either side, the spherical detection method would merely indicate that the vortex is below or above the blade. The exact spanwise location at which the vortex actually intersects the blade is not determined in this method.

In addition to the location of blade-vortex interactions on the disk (expressed in terms of the distance, r_{mid}, between the blade and the striking vortex), the angle of these interactions is a critical parameter. It is known that if the striking vortex is parallel to the blade, high noise and vibrations will ensue due to impulsive change in loading over a large portion of the blade span. On the other hand, if the striking vortex is perpendicular to the blade, the interaction results only in a spanwise change in loading (rather than a temporal or impulsive change in loading). The angle of interaction, Λ, is defined as the angle between the striking vortex segment and the blade, projected on a plane perpendicular to the rotor shaft. A parallel interaction would correspond to a value of $\Lambda = 0°$ or $180°$, and a perpendicular interaction would correspond to a value of $\Lambda = 90°$ or $270°$. On Fig. 9, the absolute value of the cosine of Λ is presented corresponding to every BVI event recorded on Fig. 8. Thus, when $\cos(\Lambda) \approx 1$, this indicates a parallel interaction (denoted by red). Conversely, when $\cos(\Lambda) \approx 0$, this indicates a perpendicular interaction (denoted by blue). Figure 9 reaffirms that the interactions I, II, and III, on the advancing side, and interactions IV and V on the retreating side are parallel, with the interactions II and V being the most parallel.

Figures 10a and 10b, respectively, shows the blade-vortex interactions predicted using the spherical detection method implemented on the moderate-resolution mesh comprising of $N_{trim} = 160$ azimuthal grid points, and on the low-resolution mesh comprising of $N_{wake} = 80$ azimuthal grid points. From Figs. 8 and 10 it is seen that with as few as 80-160 azimuthal grid points, the spherical method very effectively detects the parallel interactions on the advancing and retreating sides. In contrast, the planar detection method had considerable difficulty in identifying the parallel BVI when 80 or 160 azimuthal points were used. Since the low-resolution or moderate-resolution mesh appears viable in BVI detection using the spherical method, the requirement for interpolation of wake geometry to the grid-points of the high-resolution mesh is alleviated. Additionally, since the distance, r_{mid}, between the mid-point of a tip-vortex segment and a given control point has already been calculated at every grid point of the moderate-resolution (160 point) mesh during blade response and trim evaluations, clearly, implementation of this BVI detection method only requires determination of whether $r_{mid} \leq \bar{r}$, and no further post-processing of the rotor-wake calculations (such as transformation of collocation points to cylindrical coordinates).

Comparison of Figs. 4 and 8 (or Figs. 5 and 10) indicates that the bands representing the passage of tip-vortices in proximity of the blade extend over a wider range for the planar detection criteria. This is due to the fact that interactions occurring within 3 chord lengths above or below the blade were recorded ($\bar{h}$ = 3 chord lengths). In contrast, control spheres of radius equal to only one chord length were used in the spherical detection criteria ($\bar{r}$ = 1 chord length). This also appears to be the reason why the perpendicular interactions on the front of the disk are not clearly detected with the spherical criteria. Figure 11 shows the BVI events recorded using the planar detection method, but with $\bar{h}$ = 1 chord length. In this case it is seen that bands representing the passage of tip-vortices in proximity of the blade do not extend over quite as wide a range (compared to Fig. 4) and appear more similar to those obtained using the spherical method (Fig. 8).

Comparing Figs. 8 and 9 to Fig. 4 indicates that the planar detection method does not record the interaction V on the retreating side of the disk between 60% and 80% of the blade span. Figure 9 clearly indicates that this is a very parallel interaction, reiterating the earlier

observation that the planar detection method has maximum difficulty in identifying the occurrence of the most parallel interactions (even with the high resolution azimuthal grid used in Fig. 4). If the planar detection method is implemented using a moderate-resolution grid (Fig. 5a), the parallel interaction V is even less identifiable, and the parallel interaction II on the advancing side is no longer clearly identifiable either. When the low-resolution grid (Fig. 5b) is used, the interactions II and V are not detected at all by the planar detection method.

The spherical detection method is able to identify the occurrence of parallel BVI using even moderate- or low-resolution grids. With either of these grids, no wake geometry interpolation or post-processing of wake data is required. The computational effort is thus considerably lower than that required for the planar detection method.

6. Inflow and Blade Loads

Physically, the presence of tip vortices in proximity of the blades would have a strong influence on the induced velocity at the blade, and thus the blade loading. The induced velocities and the blade loads are calculated at the control points at several azimuthal locations as a part of the coupled blade response, trim, and free-wake evaluation process.

To identify parallel BVI, one approach that is widely used is to examine the inflow or blade loads, versus azimuth, at specified spanwise locations (for example, Refs. [9, 10]). If a parallel BVI occurs, it is expected to produce an impulsive change in inflow and blade loading at the corresponding azimuthal stations.

Figures 12 and 13 show the inflow and blade loads at a spanwise station corresponding to 80% of the blade radius. From Figs. 4 and 8 it is already known that parallel blade-vortex interactions occur on both the advancing and retreating side at this spanwise location. However, no impulsive changes in either inflow or blade sectional lift are observed in Figs. 12 and 13. This observation is consistent with Ref. [9] in which it was reported that the Maryland Free Wake analysis (on which the code used in the present study is based) was unable to predict the high-frequency BVI loading that was observed experimentally, and predicted by other analyses such as CAMRAD and 2GCHAS with the Scully wake. The lower 6 - 16 harmonics of inflow or blade loads are often filtered to obtain a clearer picture of the high-frequency BVI loading (for example, Ref. [11, 12]). However, even after filtering out the lower harmonics, no impulsive changes in inflow or loads were discernible, on either the advancing or retreating side.

Figure 14 depicts the inflow at the blade as it undergoes one revolution, with the different contours representative of different values of inflow. It would be expected that the presence of a vortex in proximity of the blade would produce a large inflow gradient, and thus a high concentration of lines on the figures. It should be emphasized that Fig. 14 does not provide a snapshot of the inflow at the rotor disk at a given instant with the rotor blade frozen at a particular azimuth (as was presented, for example, in Ref. [13], Fig. 12). Rather, as the blade undergoes one revolution, *the inflow at the blade at every azimuthal station* is recorded and plotted on the figure. Such an approach is more meaningful in identifying the occurrence of BVI as it is the inflow *at the blade* that will change when a vortex comes in proximity of the blade. The inflow over the entire disk with the blade frozen at one azimuth cannot really be used to draw any conclusions about the occurrence of BVI over the rotor disk. Similarly, Fig. 15 depicts the lift as the blade undergoes one revolution. With Figs. 14 and 15 generated as described above, "opening out" the annular ring at 80% spanwise location would produce Figs. 12 and 13. From Figs. 14 and 15, no parallel BVI on either the advancing or retreating side are detected.

7. Inflow and Blade Loads using Different Core Growth Rates

The results presented in the previous section indicated that parallel BVI events could not be detected based on the inflow or blade loads. Yet, BVI detection based on inflow or blade loads is fairly common, (for example, Refs. [6, 9-12]). This section seeks to resolve this apparent discrepancy. It is hypothesized that

the absence of any impulsive changes in inflow or blade loads in the previous section might be due to a vortex diffusion that was too large. If the vortex core radius is allowed to grow too large, the peak velocity induced by the vortex (which is almost inversely proportional to the vortex core radius) can be significantly decreased. The combination of these two related factors - *(i)* increase in core radius; and *(ii)* decrease in peak velocities, can drastically reduce the severity of the impulsive changes in inflow and loads that are normally associated with BVI. Additionally, the peak velocities induced by the vortex may have decreased to an extent that they may now be comparable to, or even much smaller than, the mean rotor inflow. Thus, they would produce only small changes in the inflow at the blade (relative to the mean) over an increased time interval, rather than the sharp changes over a small interval that have come to be associated with BVI. To examine the veracity of this hypothesis regarding the role of the vortex core size, the inflow and blade loads are re-examined in the present section using different core sizes.

The previous results presented were all obtained assuming that the vortex core radius grew as described in Eq. 1, with a value of turbulent viscosity factor, δ, of the order of 10^4 (obtained using Eq. 2 with $a_1 = 10^{-1}$). In the present section, the following additional values of the empirical parameter, a_1, corresponding to smaller vortex core growth rates are considered: $a_1 = 10^{-2}$ (corresponding to δ of the order of 10^3), and $a_1 = 10^{-3}$ (corresponding to δ of the order of 10^2). Finally, a vortex of constant core radius (r_c = 0.2 chords) is also considered. A constant core radius of 0.2 - 0.25 chords is commonly used in the literature (for example, Ref. [11, 12]). Figure 16 shows the vortex core radius as a function of wake age (in number of revolutions), for the cases $a_1 = 10^{-1}$ (baseline), $a_1 = 10^{-2}$, and $a_1 = 10^{-3}$. Also shown on the figure, for comparison, is a vortex with a constant core radius of 0.2 chords. It should be pointed out that the parallel interactions, I, II, and III, on the advancing side (see Fig. 4) occur at approximate wake ages of 1 and 1/4 revolution, 1 and 1/2 revolution, and 1 and 3/4 revolution, respectively. From Fig. 16 it can be seen that core radius between 1 and 2 rotor revolutions, is approximately 0.4 chords when $a_1 = 10^{-3}$ (δ of the order of 10^2), between 1.1 and 1.3 chords when $a_1 = 10^{-2}$ (δ of the order of 10^3), and in the range of 4 chords when $a_1 = 10^{-1}$ (δ, of the order of 10^4). Clearly, when $a_1 = 10^{-1}$, the vortex core radius is 10 times larger than the core radius obtained with $a_1 = 10^{-3}$. The peak induced velocities in this case would be only one tenth of those obtained with $a_1 = 10^{-3}$.

Figures 17, 18, and 19, respectively, depict the inflow at the blade as it undergoes one revolution, for the cases $a_1 = 10^{-2}$, $a_1 = 10^{-3}$, and $r_c = 0.2$ chords. For the case $a_1 = 10^{-2}$ (Fig. 17), only the faintest traces of the parallel interactions on the advancing and retreating sides begin to appear. Knowing that parallel BVI events occur at specific locations, it is possible to correlate that information to certain contours seen on Fig. 17. However, if this information was unavailable, it would be difficult to use Fig. 17 to identify the occurrence of parallel interactions. However, for $a_1 = 10^{-3}$ (Fig. 18) and $r_c = 0.2$ chords (Fig. 19), all the parallel interactions can be clearly identified. The lower harmonics of inflow are commonly filtered out so that the occurrence of parallel BVI is even more easily discernible [11]. Figure 20 shows the higher harmonics of inflow at the blade (7th harmonic and upward), for the case $a_1 = 10^{-3}$. Comparing to Fig. 18, it is seen that lower harmonic variations in inflow are less evident in Fig. 20 (as expected), so that the parallel BVI events can be seen more clearly.

Figure 21 shows the inflow predictions at a spanwise location of 80% of the radius, with vortex core radii corresponding to $a_1 = 10^{-1}$, $a_1 = 10^{-2}$, and $a_1 = 10^{-3}$. High frequency impulsive changes in inflow are clearly visible for the $a_1 = 10^{-3}$ case. For the lower values of a_1, the vortex core-radius is too large, and the peak velocities too low, to produce any impulsive changes in inflow.

Figures 22, 23, and 24, respectively, depict the blade lift as it undergoes one revolution, for the cases $a_1 = 10^{-2}$, $a_1 = 10^{-3}$, and $r_c = 0.2$ chords. For the case $a_1 = 10^{-2}$ (Fig. 22), the parallel interactions on the advancing and

retreating sides are not detected. However, for $a_1 = 10^{-3}$ (Fig. 23) and $r_c = 0.2$ chords (Fig. 24), the parallel interactions can be identified. Figure 25 shows the higher harmonics of lift (7th harmonic and upward) for the case $a_1 = 10^{-3}$. Comparing to Fig. 23, it is seen that lower harmonic variations in lift are less evident in Fig. 25 (as expected), and the parallel BVI events can be seen much more clearly.

For any given value of a_1, parallel blade-vortex interactions can be detected more clearly by examining inflow as compared to blade lift (compare Figs. 18 and 23, for example, for $a_1 = 10^{-3}$). This should be expected as the vortex causes a direct change in inflow, but affects the lift only via change in angle of attack. However, filtering of lower harmonics of blade loads is more beneficial than filtering of lower harmonics of inflow. The parallel BVI on Fig. 25 is much clearer than the parallel BVI on Fig. 23. In contrast, the parallel BVI seen on Fig. 20 is only slightly clearer than that on Fig. 18. Thus, when detection of BVI is based on based on blade loads, it is useful to filter the lower harmonics. For detection based on inflow at the blade, filtering the lower harmonics is seen to have less significance.

Figure 26 shows the lift predicted at 80% of the blade radius, with vortex core radii corresponding to $a_1 = 10^{-1}$, $a_1 = 10^{-2}$, and $a_1 = 10^{-3}$. High frequency impulsive changes in lift are clearly visible for the $a_1 = 10^{-3}$ case. For the lower values of a_1, the vortex core-radius is too large, and the peak velocities too low, to produce any impulsive changes in lift.

The results presented in the current section, as well as those in section 7, clearly indicate that vortex core radius is an important parameter for BVI detection based on inflow or lift. Most of the previous studies that were successful in identifying parallel BVI based on inflow or blade loads used a vortex of a small and constant core, typically 0.2 - 0.25 chords (for example, Ref. [11]). However, experimental tests have indicated that the vortex core does indeed grow with time. In Ref. [14] a turbulent viscosity factor of $\delta \approx 10$ was reported based on model rotor tests. It was mentioned, however, that for larger models, and for full-scale rotors, δ would be considerably larger. In Refs. [2, 3], a value of $\delta \approx 10^4$ was recommended based on the similarities between the predicted and experimentally measured distorted vortex geometry. It now appears that this value of δ ($a_1 = 10^{-1}$) may be too large, and a value of $a_1 \approx 10^{-3}$ ($\delta \approx 10^2$) may be a better choice. For $a_1 = 10^{-3}$, the vortex core was approximately 0.4 chords between 1 and 2 revolutions. It should be noted that the vortex core was experimentally measured for the advancing side blade-vortex interactions in the HART test, and was found to be about 0.35 chords. The selection of vortex core growth rate parameters, δ or a_1, based on distorted geometry appears to be a somewhat crude approach. In the absence of data on vortex core size, it is recommended that experimental data for blade loads (or inflow at the blade, if available) be used to select the value of the turbulent viscosity coefficient, δ (or a_1). In Figure 26, the magnitude of the peaks of the impulsive change in lift seen for $a_1 = 10^{-3}$ changed significantly as a_1 was changed. Experimental data for airloads would thus be a good source to select core size parameters.

All the BVI detection results in sections 6 and 7 based on inflow and blade loads were generated using the high-resolution BVI mesh with $N_{BVI} = 640$ grid points. Figure 27 shows the inflow as the blade undergoes one revolution, based on a moderate-resolution (160 point) grid. A value of $a_1 = 10^{-3}$ was used for this figure. Figure 28 shows the inflow at a spanwise location of 80% of the radius using the high-resolution and moderate-resolution, grids. It is seen from Figs. 27 and 28 that the moderate-resolution grid successfully identifies parallel BVI. If the moderate-resolution grid is used to detect parallel BVI - *(i)* no interpolation of wake geometry to the high-resolution grid is required, and *(ii)* no post-processing of wake data is required, since the inflow and airloads are already calculated at every point of the moderate-resolution grid as part of the blade response and trim calculations. Figure 29 shows the airloads at a spanwise location of 80% of the radius, using the high-resolution and moderate-resolution grids. While the moderate-resolution grid is able to identify the occurrence of parallel BVI, the peaks of the impulsive changes in lift are considerably

smaller than those predicted using the high-resolution grid. If BVI predictions are based on a moderate-resolution grid, inflow rather than airloads, may more accurately reflect the severity of the event (based on results shown in Figs. 28 and 29).

If the vortex core is not too diffused, BVI detection based on inflow or blade loads results in a maximum density of contour lines in regions where the miss-distance is the smallest (compare, for example, Figs. 20 and 25 to Fig. 4). This should be expected. It appears slightly easier to detect parallel BVI based on inflow rather than blade loads. However, the blade loads would be useful in an acoustic analysis.

8. Blade Root Loads

Figure 30 shows the blade root vertical force, versus azimuth, for a vortex core corresponding to $a_1 = 10^{-3}$. The blade root vertical force at any azimuthal station is obtained by the spanwise integration of the blade lift. As compared to the results obtained using a Drees inflow model, or a prescribed wake, impulsive changes in blade root loads at the azimuthal locations where BVI is known to occur are clearly observed with the free-wake. Figure 31 shows the blade root loads obtained using free-wake predictions with 3 different values of vortex core radius, corresponding to $a_1 = 10^{-1}$, $a_1 = 10^{-3}$, and $r_c = 0.2$ chords. From the figure it is observed that when the vortex core is too large ($a_1 = 10^{-1}$), the impulsive changes in blade root loads are diminished. With $a_1 = 10^{-1}$, it would be difficult to identify the occurrence of BVI on the advancing and retreating sides, without *a priori* knowledge of the event. For $a_1 = 10^{-3}$, and $r_c = 0.2$ chords, detection of parallel BVI events based on blade root loads appears possible. This is somewhat surprising as it was expected that impulsive changes in lift would be smeared due to integration along the span and the obliqueness of the interactions.

9. Concluding Remarks

In the present study BVI predictions using five different approaches were compared,. The approaches examined were - *(i)* planar detection method, *(ii)* spherical detection method, *(iii)* inflow, *(iv)* blade loads, and *(v)* blade root loads. From the results reported, the following conclusions can be drawn:

The planar detection method is inherently ill-suited for detection of parallel BVI. The method requires considerable post-processing and a very high-resolution azimuthal discretization. It clearly has considerable difficulty in detecting the occurrence of the most parallel BVI events. If the resolution of the azimuthal mesh is decreased, parallel interactions may not be detected at all. The computational overhead required is the largest of all the methods considered in this study. The planar detection method is well suited for detecting perpendicular interactions, but these are of relatively little interest.

The spherical detection method is very well-suited for detection of parallel BVI. The method was successful in detecting parallel BVI even with moderate- or low-resolution azimuthal meshes. With these meshes, no computational overhead associated with wake geometry interpolation or post-processing, of any kind, is required.

When inflow at the blade, or blade lift, is used to identify blade-vortex interactions, the vortex core model used is very important. If the vortex core grows too quickly (resulting in a significant decrease in the peak velocities) no impulsive change in inflow or loads is discernible. It is recommended that experimental airloads data (rather than wake geometry) be used to select the parameters that control core-size or core-growth. If the vortex is sufficiently "tight" parallel interactions can be clearly identified based on either the inflow or blade lift. This appears to be true even when the moderate-resolution grid is used. If the moderate-resolution grid is used, no computational overhead associated with wake geometry interpolation or post-processing of wake data is involved. When using a moderate-resolution grid, the peaks of the impulsive changes in inflow are captured more accurately, whereas the peaks of impulsive changes in loads may be underpredicted, somewhat. If detection of parallel BVI is based on blade loads, filtering the lower harmonics of blade loads enables easier identification of the interaction. For

detection based on inflow, filtering the lower harmonics has less of an influence.

When the vortex core is sufficiently "tight", impulsive changes in blade root loads are obtained at azimuthal locations corresponding to the occurrence of parallel blade-vortex interactions.

References

[1] Yu, Y. H., "Rotor Blade-Vortex Interaction Noise: Generating Mechanisms and its Control Concepts," *Proceedings of the AHS 2nd International Aeromechanics Specialists' Conference*, Bridgeport, CT, Oct. 1995.

[2] Bagai, A., and Leishman, J. G., "Rotor Free-Wake Modeling using a Pseudo-Implicit Technique - Including Comparisons with Experimental Data," *Journal of the American Helicopter Society*, Vol. 40, No. 3, pp. 29-41, July 1995.

[3] Bagai, A., and Leishman, J. G., "Free-Wake Analysis of Tandem, Tilt-Rotor and Coaxial Rotor Configurations," *Journal of the American Helicopter Society*, Vol. 41, No. 3, pp. 196-207, July 1996.

[4] Tauszig, L., "Numerical Detection and Characterization of Blade-Vortex Interactions Using a Free Wake Analysis," MS Thesis, Department of Aerospace Engineering, The Pennsylvania State University, 1998.

[5] Brooks, T. F., Boyd, D. D., Burley, C. L., and Jolly, J. R., "Aeroacoustic Codes for Rotor Harmonic and BVI Noise - CAMRAD.Mod1/HIRES," *Proceedings of the 2nd AIAA/CEAS Aeroacoustics Conference*, State College, PA, May 1996.

[6] Jones, H. E., and Burley, C. L., "A Study of the Effect of Blade Shape on Rotor Noise," *Proceedings of the American Helicopter Society Technical Specialists' Meeting on Rotorcraft Acoustics and Aerodynamics*, Williamsburg, Virginia, Oct. 28-30, 1997.

[7] Lamb, Sir Horrace, "Hydrodynamics," 6th Edition, pp. 592-593, 668-669, Cambridge University Press, 1932.

[8] Martin, R. M., Elliott, J. W., and Hoad, D. R., "Experimental and Analytical Predictions of Rotor Blade Vortex Interaction," *Journal of the American Helicopter Society*, Vol. 31, No. 4, pp. 12 - 20, Oct. 1986.

[9] Lim, J. W., and Tung, C., "2GCHAS Predictions of HART Blade-Vortex Interaction Loading," *Proceedings of the American Helicopter Society Technical Specialists' Meeti-ng on Rotorcraft Acoustics and Aerodynamics*, Williamsburg, Virginia, Oct. 28-30, 1997.

[10] Tung, C., Gallman, J., Kube, R., Wagner, W., van der Wall, B., Brooks, T., Burley, C., Boyd, D., Rahier, G., and Beaumier, P., "Prediction and Measurement of Blade-Vortex Interaction Loading," *Proceedings of the 1st Joint CEAS/AIAA Aeroacoustics Conference*, Munich, Germany, June 1995.

[11] Van der Wall, B., and Roth, M., "Free Wake Validation on Massively Parallel Computers and Validation with HART Test Data," *Proceedings of the 53rd Annual Forum of the American Helicopter Society*, Virginia Beach, Virginia, April 29 - May 1, 1997.

[12] Marcolini, M. A., Martin, R. M., Lorber, P. F., and Egolf, A. T., "Prediction of BVI Noise Patterns and Correlation with Wake Interaction Locations," *Proceedings of the 48th Annual Forum of the American Helicopter Society*, Washington DC, June 1992.

[13] Bagai, A., Leishman, J. G., and Park, J., "A Free-Vortex Rotor Wake Model for Maneuvering Flight," *Proceedings of the American Helicopter Society Technical Specialists' Meeting on Rotorcraft Acoustics and Aerodynamics*, Williamsburg, Virginia, Oct. 28-30, 1997.

[14] Leishman, J. G., Baker, A., and Coyne, A., "Measurements of Rotor Tip Vortices Using Three-Component Laser Doppler Velocime-try," *Proceedings of the AHS 2nd International Aeromechanics Specialists' Conference*, Bridge-port, Connecticut, Oct. 11 - 13, 1995.

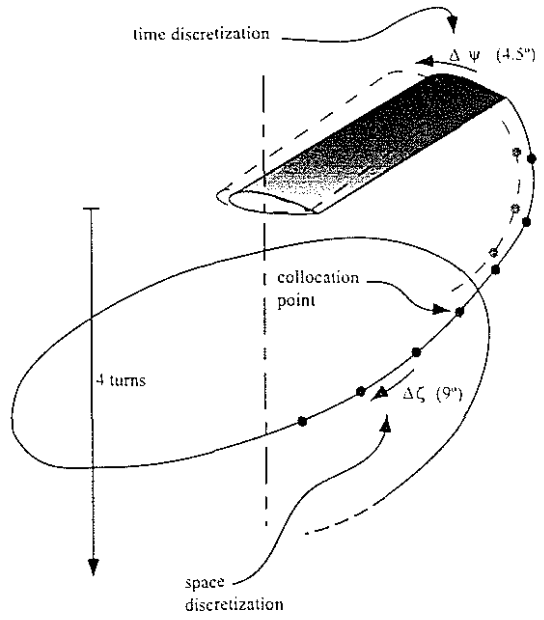

Fig. 1: Schematic representation of the wake, discretized in space and time, and extending for a finite number of revolutions below the rotor disk

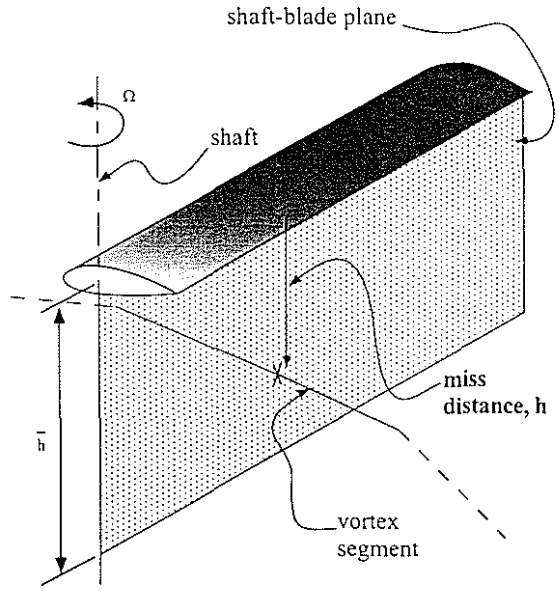

Fig. 2: In the planar detection method a BVI event is recorded when a vortex segment intersects the blade-shaft plane within a prescribed distance, $\bar{h}$, above or below the blade

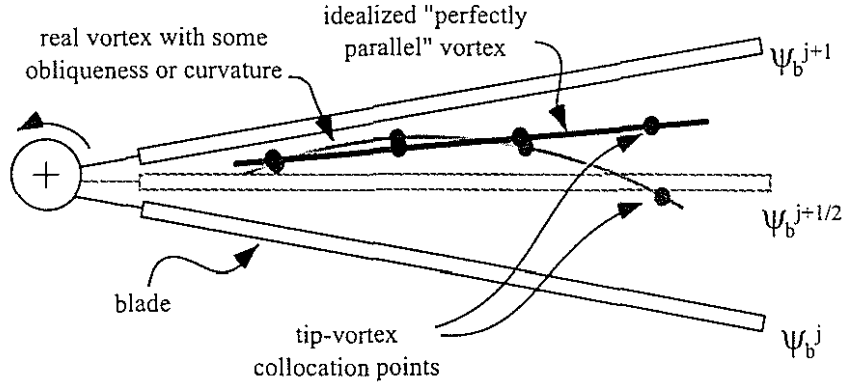

Fig. 3: Schematic sketch illustrating the inability of the planar detection method to identify the occurrence of perfectly parallel BVI events

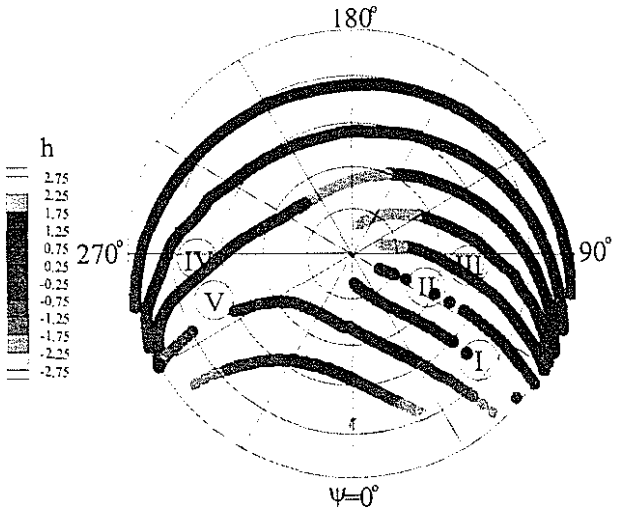

Fig. 4: Blade-vortex interactions predicted using planar detection method at 640 azimuthal grid points (of the high-resolution grid)

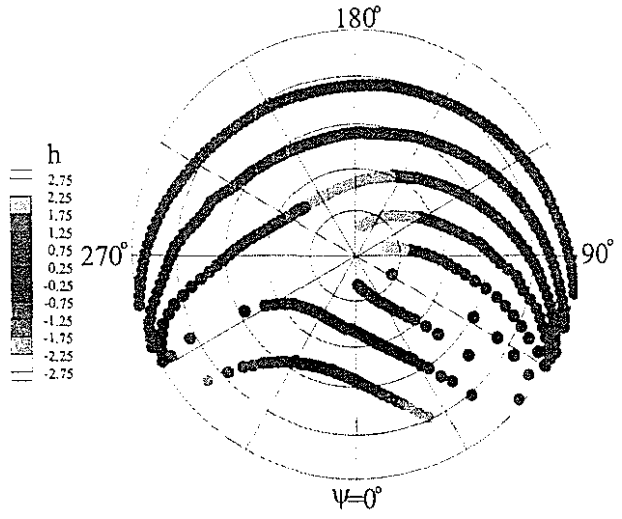

Fig. 5a: Blade-vortex interactions predicted using planar detection method at 160 azimuthal grid points (of the moderate-resolution grid)

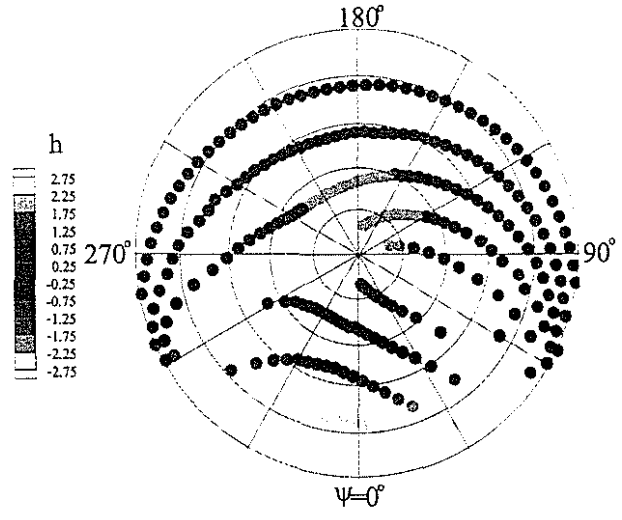

Fig. 5b: Blade-vortex interactions predicted using planar detection method at 80 azimuthal grid points (of the low-resolution grid)

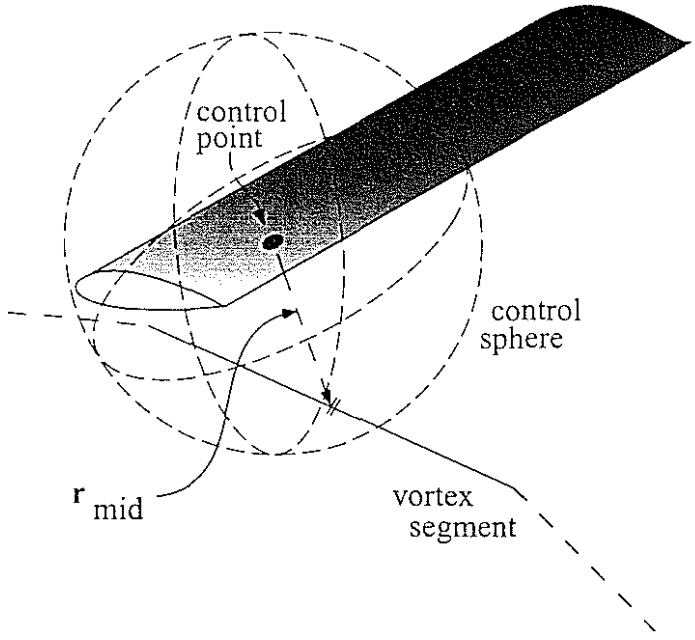

Fig. 6: In the spherical detection method a BVI event is recorded when the mid-point of a vortex segment falls within one of the control spheres (of prescribed radius $\overline{r}$) on the blade

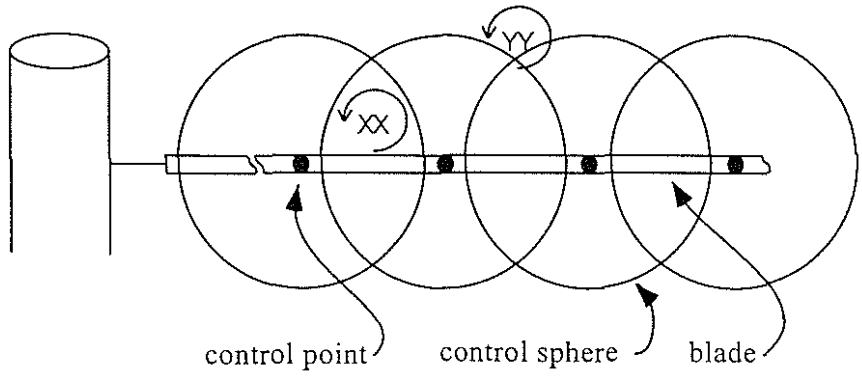

Fig. 7a: Schematic sketch illustrating the overlapping control spheres of the spherical detection method alleviating discretization errors in the spanwise direction

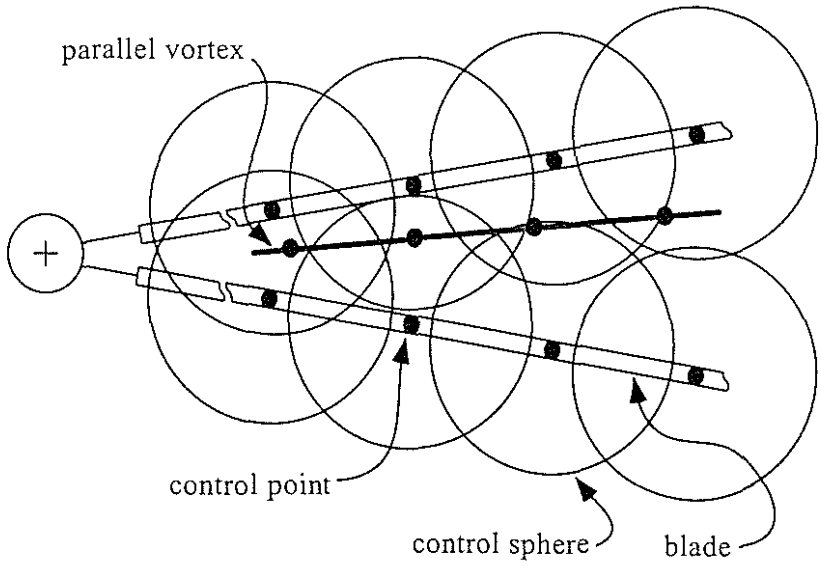

Fig. 7b: Schematic sketch illustrating the overlapping control spheres of the spherical detection method alleviating discretization errors in the azimuthal direction

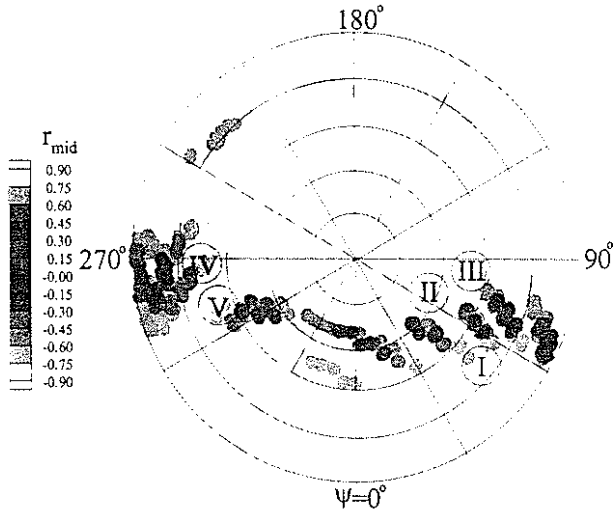

Fig. 8: Blade-vortex interactions predicted using spherical detection method at 640 azimuthal grid points (of the high-resolution grid)

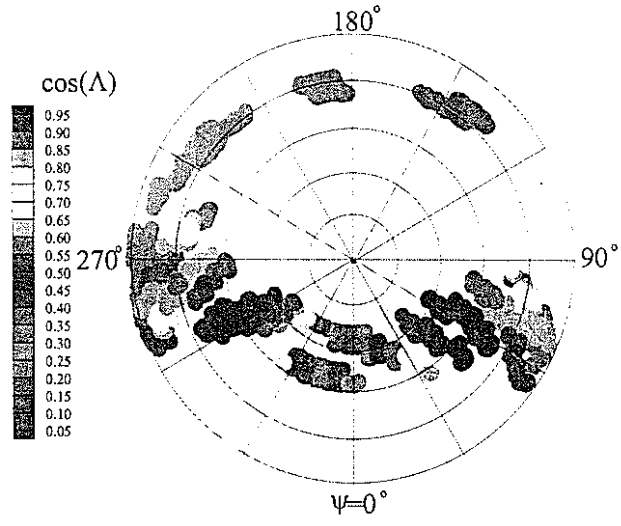

Fig. 9: Angle of the BVI events predicted in Fig. 8

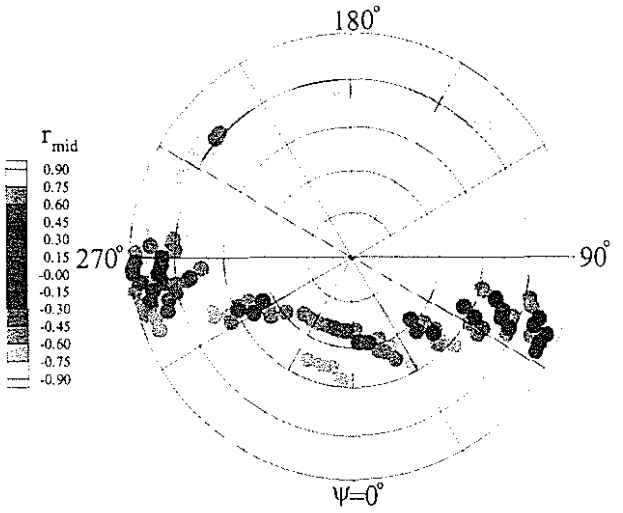

Fig. 10a: Blade-vortex interactions predicted using spherical detection method at 160 azimuthal grid points (of the moderate-resolution grid)

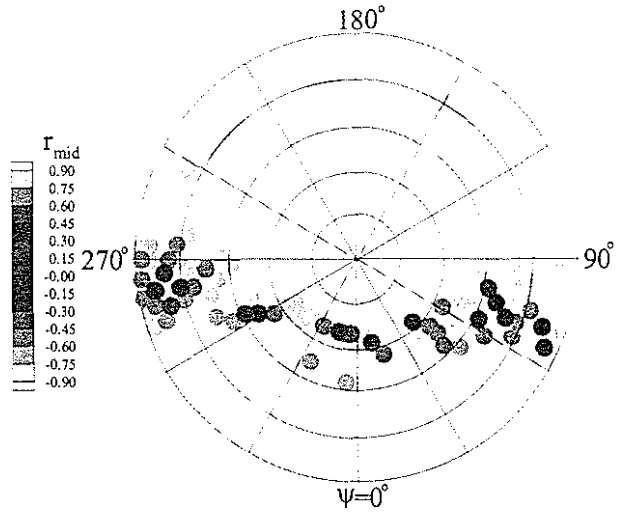

Fig. 10b: Blade-vortex interactions predicted using spherical detection method at 80 azimuthal grid points (of the low-resolution grid)

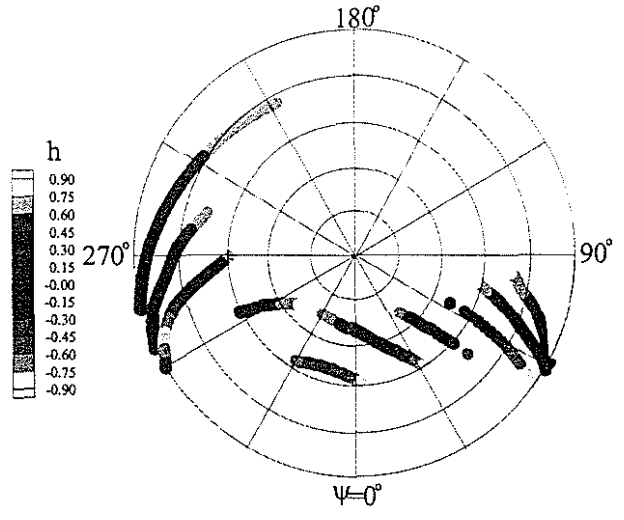

Fig. 11: Blade-vortex interactions predicted using planar detection method at 640 azimuthal grid points, with $\overline{h}$ = 1 chord length

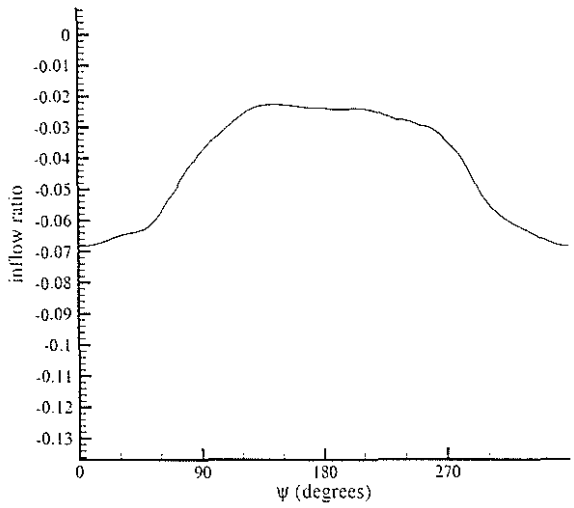

Fig. 12: Variation of inflow at the blade versus azimuth (at r/R = 0.8)

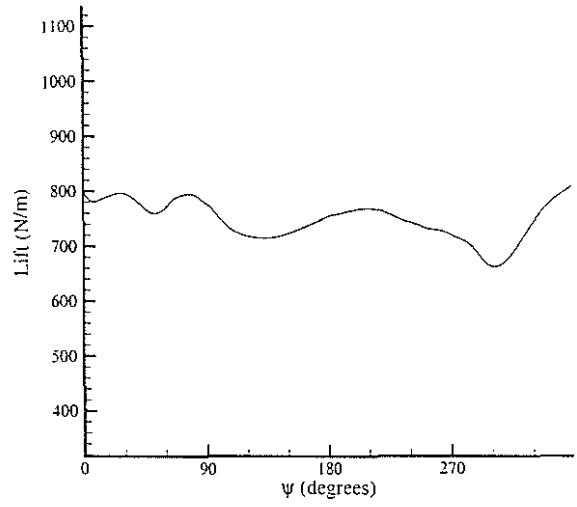

Fig. 13: Variation of blade lift versus azimuth (at r/R = 0.8)

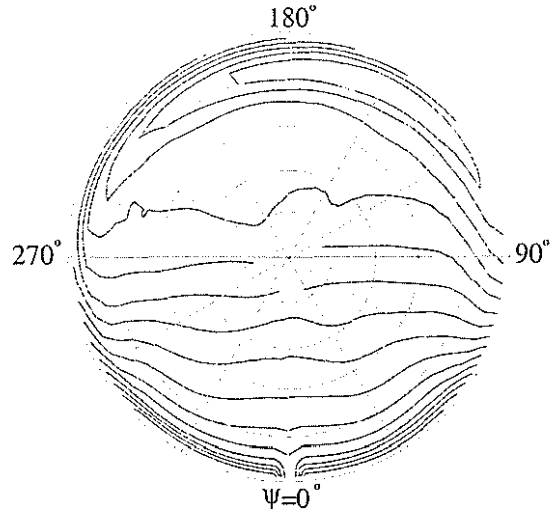

Fig. 14: Inflow at the blade over one revolution

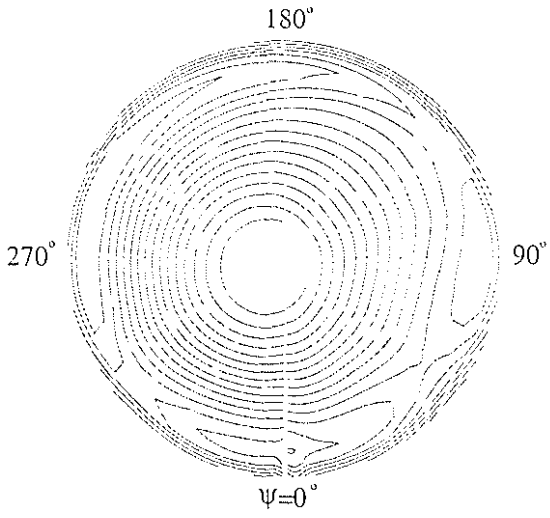

Fig. 15: Blade lift over one revolution

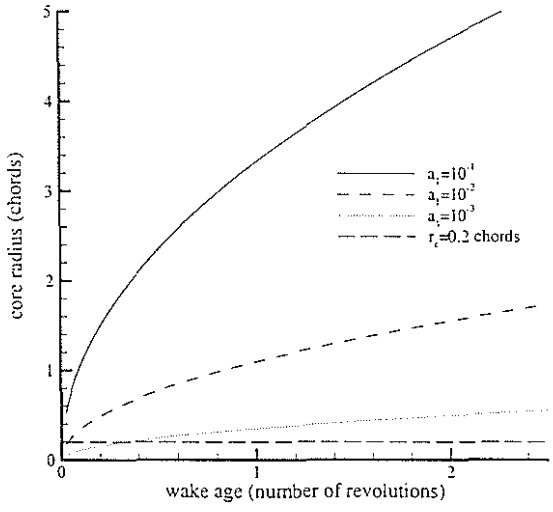

Fig. 16: Vortex core radius as a function of wake age (in number of revolutions) for different growth rates (corresponding to different values of a_i)

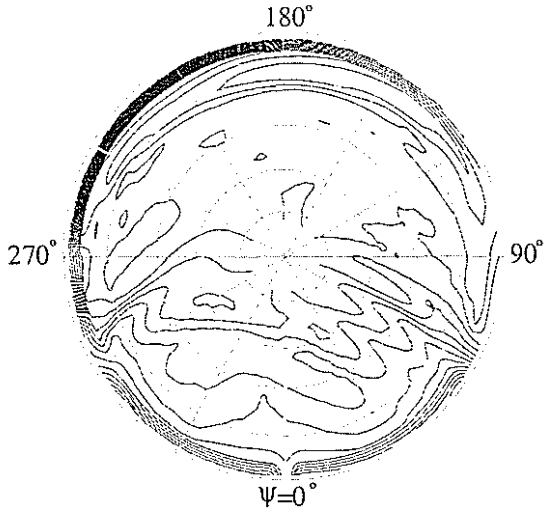

Fig. 17: Inflow at the blade over one revolution ($a_i=10^{-2}$, δ of the order of 10^3)

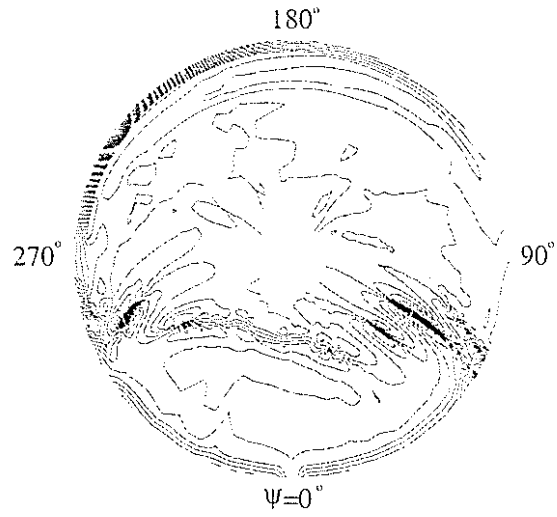

Fig. 18: Inflow at the blade over one revolution ($a_1=10^{-3}$, δ of the order of 10^2)

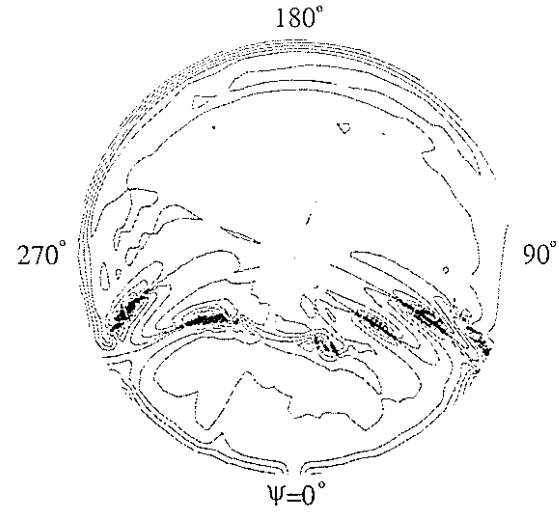

Fig. 19: Inflow at the blade over one revolution (r_c= 0.2 chords)

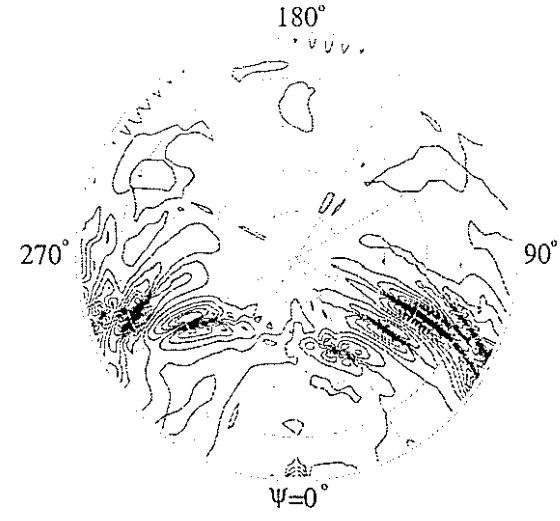

Fig. 20: Inflow at the blade over one revolution, lowest 6 harmonics filtered ($a_1=10^{-3}$, δ of the order of 10^2)

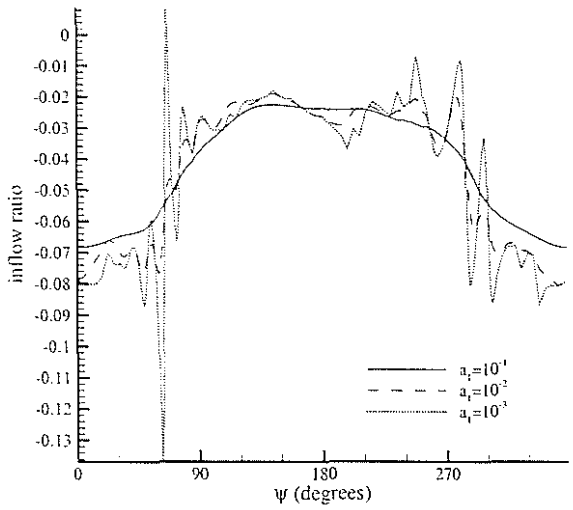

Fig. 21: Variation of inflow at the blade versus azimuth (at r/R = 0.8) for core radius parameters $a_1=10^{-1}$, 10^{-2}, and 10^{-3}

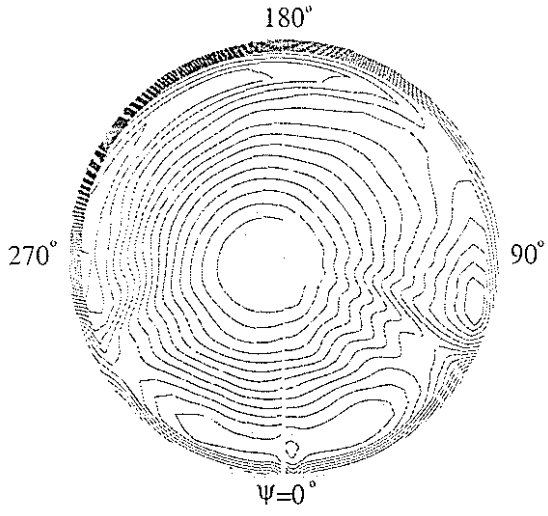

Fig. 22: Blade lift over one revolution ($a_1=10^{-2}$, δ of the order of 10^3)

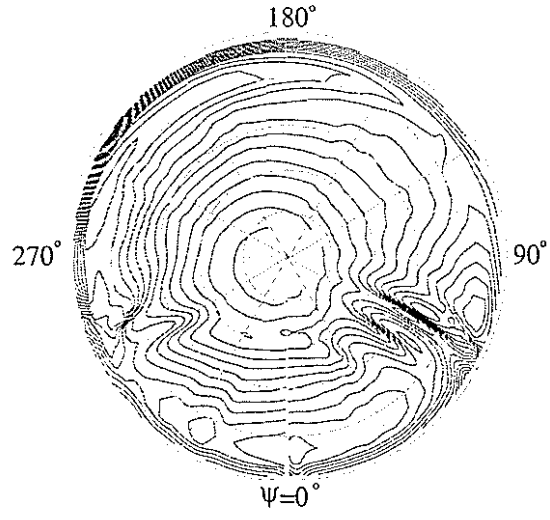

Fig. 23: Blade lift over one revolution ($a_1=10^{-3}$, δ of the order of 10^2)

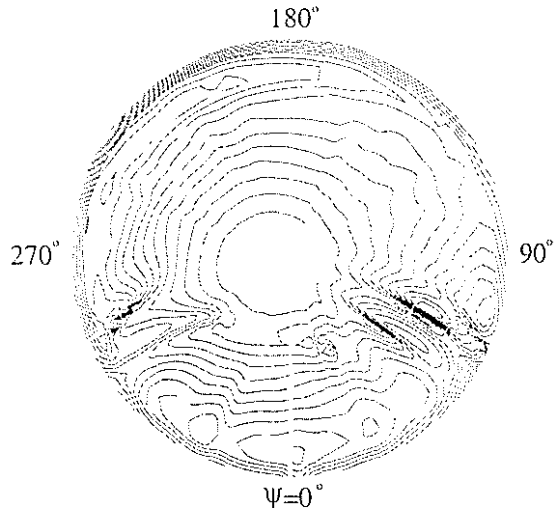

Fig. 24: Blade lift over one revolution (r_c = 0.2 chords)

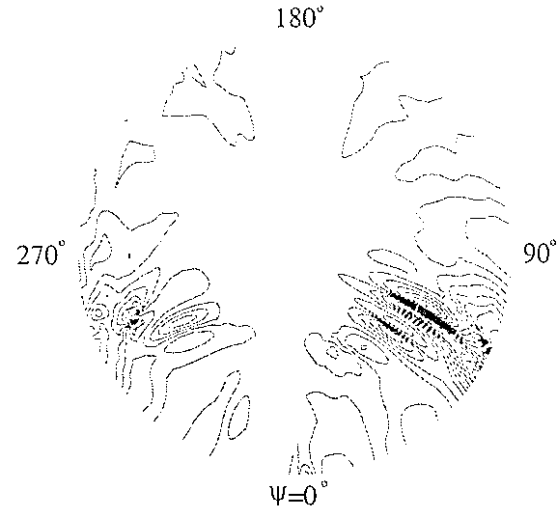

Fig. 25: Blade lift over one revolution, lowest 6 harmonics filtered ($a_1=10^{-3}$, δ of the order of 10^2)

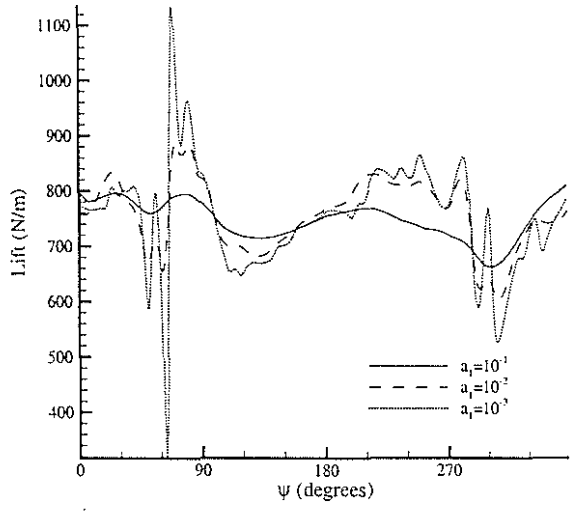

Fig. 26: Variation of blade lift versus azimuth (at r/R = 0.8) for core radius parameters $a_1=10^{-1}$, 10^{-2}, and 10^{-3}

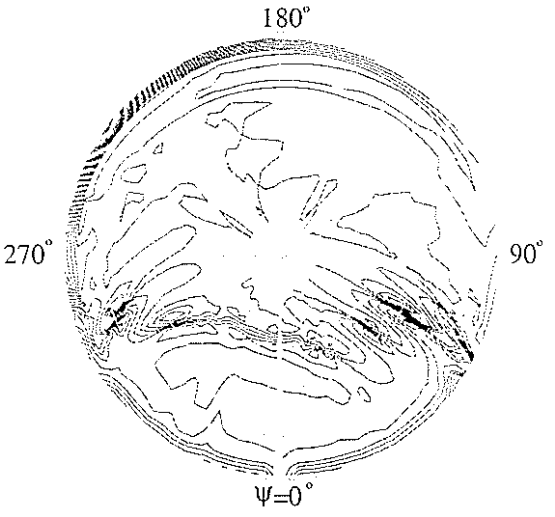

Fig. 27: Inflow at the blade over one revolution, using moderate-resolution 160-point grid (a_1=10^{-3}, δ of the order of 10^2)

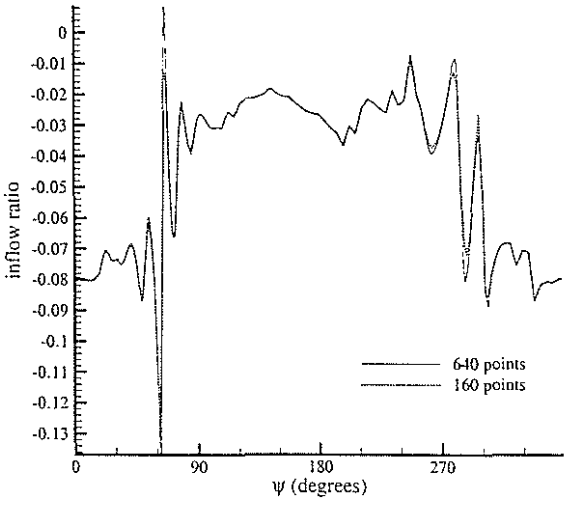

Fig. 28: Variation of inflow at the blade versus azimuth (at r/R = 0.8) obtained using high- and moderate-resolution grids (a_1=10^{-3})

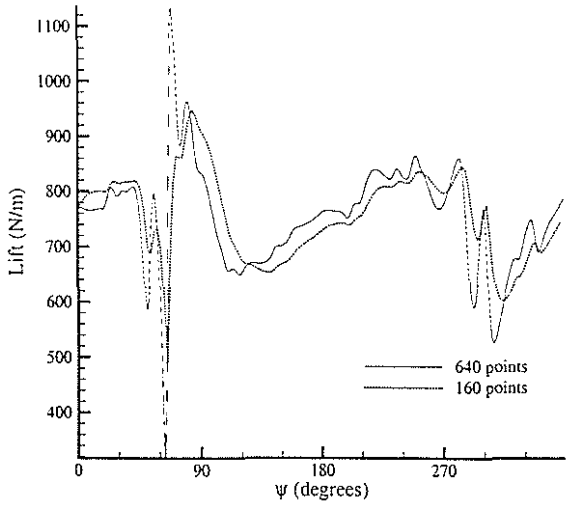

Fig. 29: Variation of blade lift versus azimuth (at r/R = 0.8) obtained using high- and moderate-resolution grids (a_1=10^{-3})

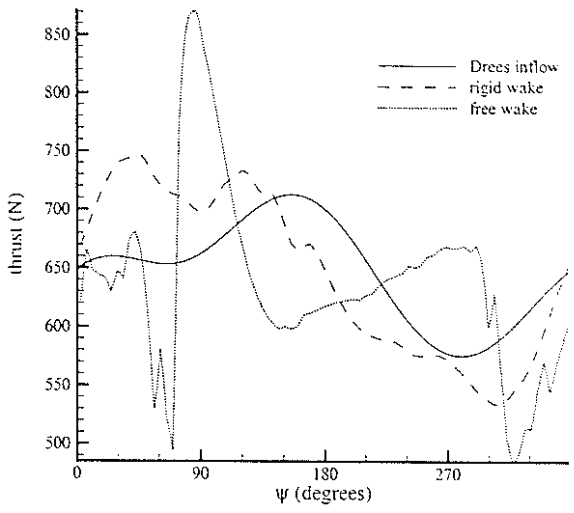

Fig. 30: Blade root vertical force versus azimuth (a_1=10^{-3})

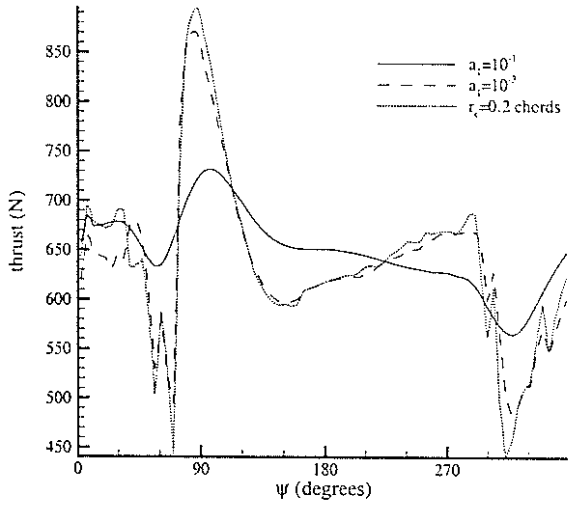

Fig. 31: Blade root vertical force versus azimuth (a_1=10^{-1}, a_1=10^{-3}, r_c=0.2 chords)